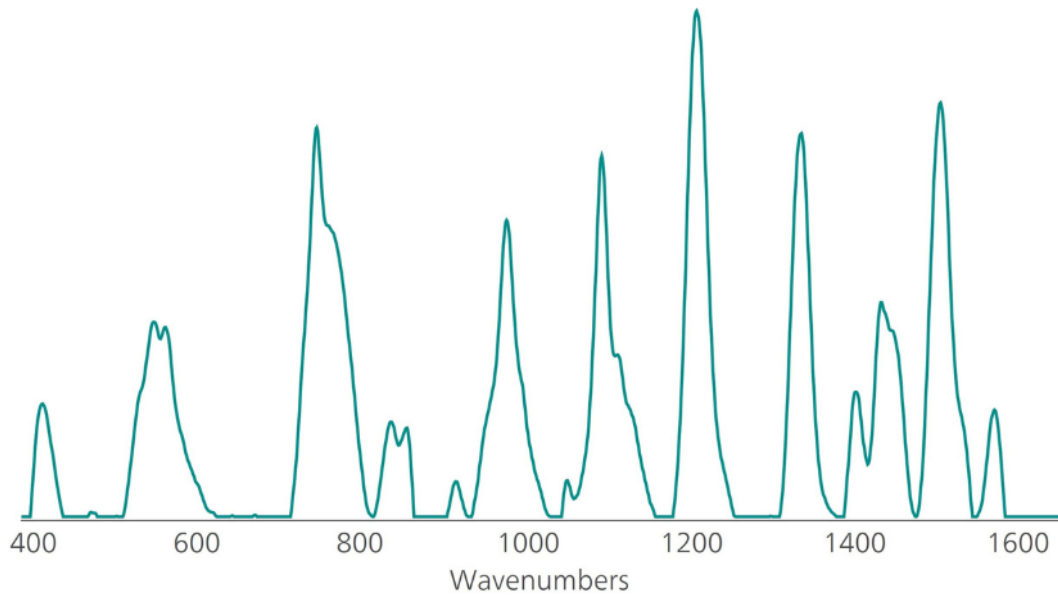
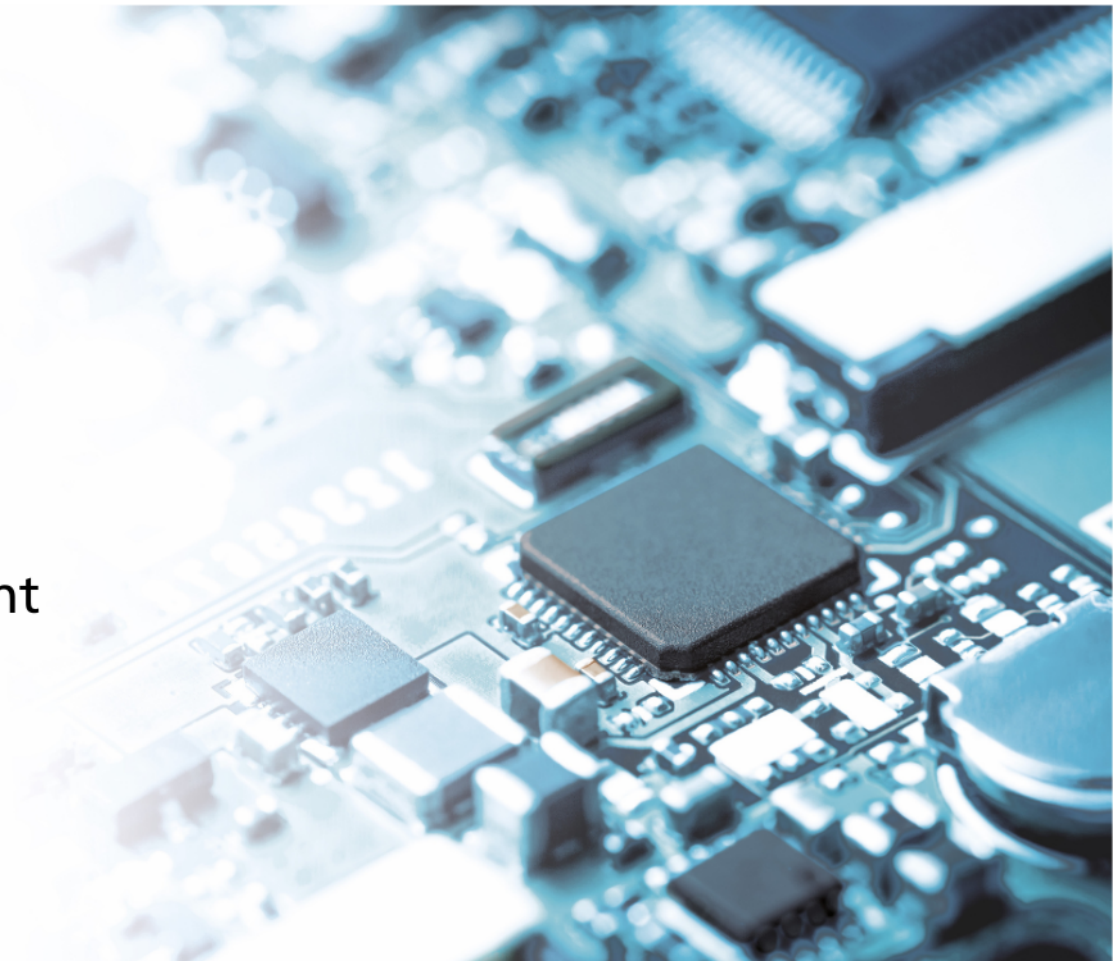




ENABLING YOUR SOLUTION



Your Trusted
Partner for
Customization
and Development



Soft Tactile Coil-Based Sensor for Misalignment Detection of Adhesive Fibrillary Gripping Systems

Simon Herter,* Philipp Stopp, and Sarah C.L. Fischer*

Micropatterned dry adhesive systems are a promising alternative to conventional handling solutions. However, the use of these gripping systems still requires precise manual adjustment of the gripping parameters. To address this limitation, a coil-based sensor is designed to enable automatic detection of the attachment process. The sensor consists of three sensing, one transmitting coil, a conductive film, and a compliant layer. The components are optimized to achieve reproducible, precise measurements, and minimize hysteresis effects of the components. A mathematical concept to calculate the geometrical relations between the gripping object and the gripper is established based on triangulation. The functionality of the sensor system is demonstrated in contact experiments with a glass substrate under different tilt angles, and an accuracy of 0.042 degree is achieved. The sensor system not only allows precise detection of the misalignment angle but also fast estimation of the qualitative direction of misalignment with minimal compression. This is interesting for scaling the sensor system to industrial pick-and-place applications as it promises to speed up the handling times and reliability of the fibrillary adhesives. In the future, the system needs to be extended to capture more complex objects and properties to be applicable to more handling problems.

polymers.^[1–3] Several approaches exist to optimize the pillars by varying their shape and material choice and utilizing composite approaches, however, the most common variant is mushroom-shaped pillars.^[4–10]

One advantage of these bioinspired structures as end effectors is energy efficiency, as they do not need any external energy source for operating. The underlying physical principle of the switchable physical adhesion mechanism are van der-Waals forces. Switching between the adhesive and non-adhesive state is realized by variations in mechanical load: a small normal force enables contact between the microstructures (attachment) and a larger normal or rotational force results in elastic instability and buckling (detachment).^[11]

The adhesion force is influenced by environmental conditions like the roughness of the object, the temperature, and the misalignment between the pillars and the object's surface.^[11–14] The principle to realize multiple pillars as an end effector

1. Introduction

Inspired by natural dry adhesives, micropatterned surfaces found their way into automated gripping solutions as novel end effectors for robotic pick-and-place applications. The functional surfaces consist of fibrillar structures, technically called pillars, ordered in patterns and commonly fabricated from soft elastic

for robotic applications is to build multiple adhesive pillars as an array (short: adhesive pad or pad) on a backing layer, which distributes the stress among the individual pillars.^[12] Due to this setup, the array of pillars is sensitive to misalignment. Kroner et al. showed that a misalignment angle of just 0.2 degrees can yield a drop of >30% in the adhesion.^[15]

Modification of the compliance of the backing layer of the pillar array is a strategy to reduce the decreasing adhesion due to misalignment.^[13,16] To modify the compliance of the backing layer, the thickness or the material can be changed, for example, by placing a foam behind the adhesive array. Modification of the backing layer is not a solution to the problem itself, therefore possibilities to detect the misalignment and correct it in an auto-adaptive manner are desirable.

For industrial handling devices based on micropatterned arrays the detection of misalignment is a key factor in increasing reliable and well-controlled manipulation processes. With a sensor capable of detecting the misalignment during the grasping of objects a feedback loop to the handling system, e.g. a robot, can be established enabling a readjustment to an optimal tilting angle (e.g., perfect planar alignment).

To solve this task there are several requirements a sensor has to fulfill. The sensor needs to be sensitive to small deformations caused by the attachment of the pillar array while not reducing

S. Herter, P. Stopp, S. C. Fischer
 Fraunhofer Institute for Nondestructive Testing IZFP
 66123 Saarbruecken, Germany
 E-mail: simon.herter@izfp.fraunhofer.de;
 sarah.fischer@izfp.fraunhofer.de

S. Herter
 Lab for Measurement Technology
 Saarland University
 66123 Saarbruecken, Germany

 The ORCID identification number(s) for the author(s) of this article can be found under <https://doi.org/10.1002/adsr.202300098>

© 2023 The Authors. Advanced Sensor Research published by Wiley-VCH GmbH. This is an open access article under the terms of the Creative Commons Attribution License, which permits use, distribution and reproduction in any medium, provided the original work is properly cited.

DOI: 10.1002/adsr.202300098

the load-bearing capability of the adhesive pad. Furthermore, the sensor should measure the deformation locally to allow for a calculation of the misalignment of the pad. Additionally, economic and application-driven factors come into play and introduce requirements like reproducibility, cost efficiency, speed, and robustness.

To implement such a deformable and tactile sensor different kinds of electrical signals like impedance, frequency, and voltage can be utilized to measure the misalignment.^[17–20] Additionally magnetic- and optic measurement techniques can be exploited.^[21–24] Magnetic and capacitive transducers are sensitive and fast but suffer from external influences like contamination or magnetic fields.^[19,25–27] Capacitive sensors in particular have been considered in current research to create soft tactile sensor designs for wedges-shaped adhesives.^[29–33] Eddy current sensors, which are widespread in industrial applications, were recently shown to have the potential to overcome those limitations.^[18,19,28]

In this work, we will present a novel sensor based on the eddy current principle for detecting misalignments in the case of adhesive pads for grasping objects. A multi-coil-based sensor measuring the displacement of a conductive material relative to the sensing coils enables tilt detection. The displacement is induced by contact between the adhesive pad and the object being grasped. Subsequently, a misalignment plane can be approximated based on triangulation of the three recorded sensor signals and provides feedback for the gripping process. Contact experiments were carried out to optimize the sensor components and quantify the accuracy of the final sensor stack.

2. Results and Discussion

This research presents a novel idea for a malleable, tactile sensor for bioinspired robotic grippers to rectify misalignment during grasping operations.

First, the novel sensor principle is introduced and an optimized composition of the sensor stack is experimentally determined. Second, the sensor is evaluated on a robotic setup to characterize the capability of the sensor to determine misalignment angles of the pad with respect to a surface.

2.1. Sensor Concept and Working Principle

A concept for an eddy current-based sensor was established in this work (Figure 1). The sensor stack consists of one transmitter coil and three receiver coils. The receiver coils are placed on an equilateral triangle inside the transmitter. The three receiver coils are needed to calculate the equation of the misalignment plane based on the obtained distances at three different positions. Besides the coil system, the sensor consists of a foam connected to the printed circuit board (PCB) itself, acting as a supporting structure and a deformable spacer between the adhesive pad and the conductive measuring layer material. Figure 1a visualizes the adhesive pad system without the sensor integration and Figure 1b shows the integration of the sensor components as described.

The underlying working principle of the sensor is based on eddy currents. Transferred to the presented sensor concept the

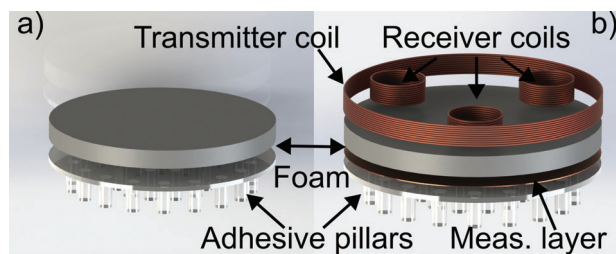


Figure 1. Tactile sensor concept and its components. a) CAD adhesive pad sample, b) CAD integrated sensor design.

transmitter coil is used to excite eddy currents in the measuring layer by sending an alternating voltage signal to the coil. The receiver coils detect a voltage change, which is generated by the eddy current-induced alternating magnetic field from the measuring layer. This detectable voltage change makes it feasible to map the voltage change to a distance variation between the measuring layer and the receiver coils. When the adhesive pads approach an object and get in contact the pressure leads to a deformation of the measuring layer as well as the foam, which results in a voltage change in the receiver coils and is the primary sensor signal of the system.

2.2. Sensor Design and Characterization

2.2.1. Analysis of the Electrical Characteristics of the System

The impedance curve as well as the scattering parameter S_{21} are measured for choosing the right excitation frequency for the system.

Figure 2 shows the results obtained from the measurements with the impedance and network analyzer in Figure 2a,b respectively. The transmitter coil shows the self-resonance peak at 1.8 MHz, regardless of how many receivers are shorted. As the transmitting coil has the lowest self-resonance of the system, it determines the upper excitation frequency. Consequently, the ideal excitation frequency of the system is below 1.8 MHz to avoid the capacitive part of the coil becoming dominant. The measurement of the self-resonance is performed with the connecting cable as it is a part of the system.

The scattering parameter S_{21} (Figure 2b) provides information of the transmission function between the transmitter and the receiver coils. For reliable signal transmission, a small damping is preferable. The lowest damping of the transmission is achieved at ≈ 460 kHz with a damping of -27.8 dB, but is only increasing to a value of -30.2 dB for 2 MHz. From the scattering parameter and the impedance analysis, an excitation frequency between 460 kHz and 2 MHz is suitable and fulfills all requirements.

A further boundary condition for selecting a proper frequency is the skin depth. To reduce influences from other conductive parts such as the measuring layer material, the skin depth should be as small as possible which favors higher frequencies. The excitation frequency is set to 1 MHz as this frequency represents a compromise between all requirements and is easily excitable via a look-up table and an internal system clock of 125 MHz.

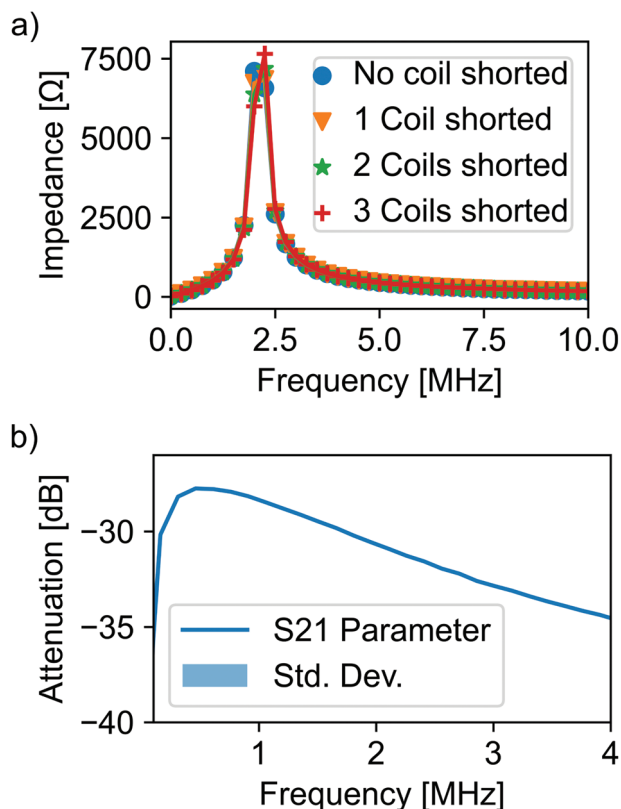


Figure 2. Electrical characterization of the sensor system. a) Impedance curve of the transmitter coil with and without shorted receivers b) Scattering parameter curve of the system.

Table 1. Averaged sensor signals for different measuring layer materials for a distance difference of 400 μm .

Measuring layer material	Averaged amplitude [digits]
3304 BCS	11441
ECATT9711S-200	8270
Shieldex Kassel	16266
Copper foil*	10770

2.2.2. Selection of the Measuring Layer Material

The key factors in selecting a suitable measuring layer material are the following two:

- 1) High conductivity for efficient excitation of eddy currents
- 2) Matching mechanical compliance of the material with respect to the adhesive system

First, the electrical properties of the measuring layer material are tested.

In **Table 1** the averaged maximal differences of the measurements can be seen. The average maximal difference is the difference between the start and end signal averaged over all three coils.

Table 2. Influences of the different components on the adhesion force.

Configuration	Normalized adhesion force	Std. Dev.
1. Pad	1.00	-
2. Pad with foam	0.81	0.01
3. Pad with Shieldex	1.06	0.03
4. Pad with foam and Shieldex	0.92	0.01

From **Table 1** it follows that the measuring layer material with the commercial designation Shieldex Kassel (Shieldex) provides the best sensor signal and outperforms the reference value of the copper foil.

Next, Shieldex is evaluated regarding the mechanical influence on the adhesive force. Therefore the four configurations, see **Table 2** are tested, each test is normalized to the respective adhesion force for the same pad (tip modified) without additional components. **Table 2** summarizes the normalized adhesion forces; the values highlight that Shieldex as a measuring layer material has no negative influence on the adhesion force especially if configurations 2 and 4 are compared.

Shieldex is selected from here on as the measuring layer for the sensor stack based on the electrical characterization.

2.2.3. Selection of the Foam

The preload-induced deformation behavior of the foam is a key factor for the sensor. A stable behavior over multiple cycles is required in order to calibrate the sensor. The shifting of the preload is determined by cyclic loading of the specimen. The preload ranges from -100 to $+100$ N for each foam specimen 50 runs are performed. The preload shift of the pressure regime is mainly interesting, because this is the general operating range of the sensor. A small preload shift is preferred so that the foam relaxation and material behavior have less influence on the deformation of the system. A high preload shift results in a large impact of the foam behavior on the sensor characteristics. The examination of the five foam specimens is shown in **Figure 3a,b**.

The samples from 3M PT1500 and the KS 865 F are of interest for the sensor design, as they show the smallest preload shift. Sample GT7116 is not suitable as the preload shift is positive which indicates a decreasing displacement and the measurement effect would decrease in the compressive state. Besides the preload shift, the absolute deformation of the foam is important as well as the hysteresis. The foam itself acts as the deformable feature in the sensor concept so the stiffness and flexibility of the foam directly correlate with the measured signal. Therefore, a soft foam will result in more displacement of the measuring layer material compared to a stiff foam. Next, the two most promising foams (3M PT1500 and KS 865 F) were evaluated with respect to their displacement curves under loading (**Figure 3b**). The hysteresis of foam sample KS 865 F shows a displacement over 1 mm whereas sample 3M PT1500 shows a displacement less than 1 mm. As large shifts provide more displacement and consequently more signal foam KS 865 F is selected as the supporting structure.

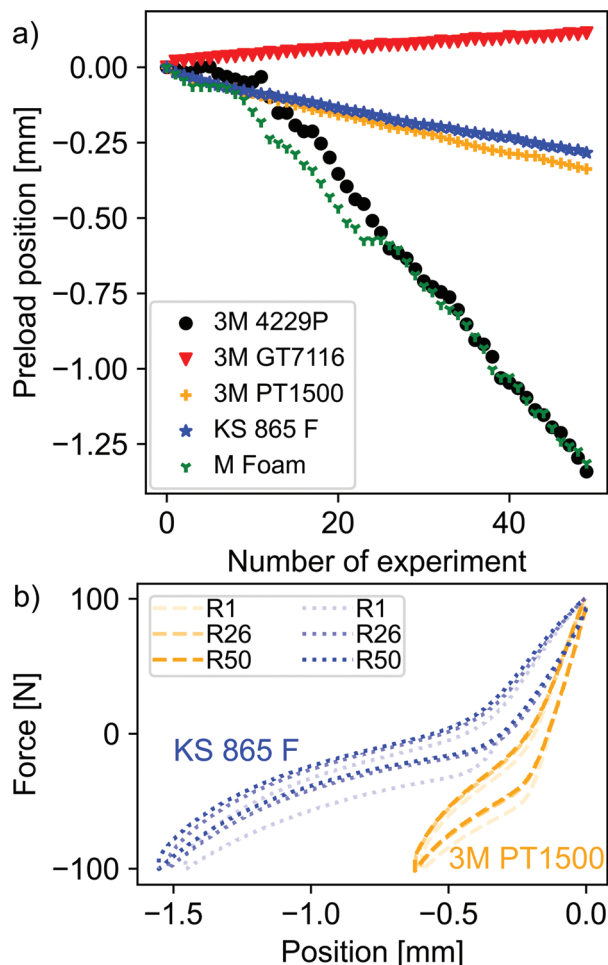


Figure 3. Mechanical characterization of the foam specimens: a) Preload position shift of the five different foam specimens. b) Hysteresis diagrams for foam sample 3M PT1500 (yellow) and KS 865 F (blue) shown for the 1th, 26th, and 50th loading cycle.

2.2.4. Final Sensor Stack and Sensor Calibration

After evaluating all components, a combination of the PCB coil sensor in conjunction with the foam KS 865 F and Shieldex in conjunction with the pad is set as the final sensor stack. This sensor stack needs to be calibrated before the tilting angles can be calculated.

For the measurement of the coil calibration curves, the measuring layer material together with the foam as supporting structure is connected to the sensing layer. This setup is then pressed against a glass substrate and a robot is moving stepwise (40 μm) closer to the glass substrate for 1 mm and this procedure is repeated six times. To prevent damage of the load cell, a force limit of 30 N was set.

The first two measurement steps are excluded from the calibration because in the first compression phase, all the single components settle and the curve could slightly deviate from the repeated measurements. In addition, the first step is not necessarily 40 μm . For the calibration process, the signal amplitude of each step is averaged and plotted against the distance **Figure 4**.

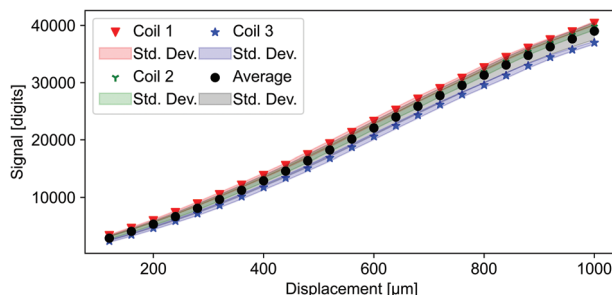


Figure 4. Calibration curves for each individual receiver coil and the averaged curve of all receiver coils.

Table 3. Calibration coefficients of the receiver coils.

a [$\mu\text{m digits}^{-3}$]	1.086×10^{-11}
Std. Dev. a [$\mu\text{m digits}^{-3}$]	1.95×10^{-12}
b [$\mu\text{m digits}^{-2}$]	-7.304×10^{-7}
Std. Dev. b [$\mu\text{m digits}^{-2}$]	1.05×10^{-7}
c [$\mu\text{m digits}^{-1}$]	0.0371
Std. Dev. c [$\mu\text{m digits}^{-1}$]	0.0021

The resulting curve is a superposition of deformation of the foam as well as the decrease of the magnitude of the magnetic field with increasing distance. Therefore, the curve is fitted with a polynomial of third degree to take into account underlying physical effects (Equation (1)):

$$f(x) = a \cdot x^3 + b \cdot x^2 + c \cdot x \quad (1)$$

All curves are averaged to obtain the calibration factors since the coils are technically identical in terms of their properties. The deviations in the individual calibration curves are due to the application of the foam and the measuring layer, as well as possible skew loads during calibration. **Table 3** summarizes all coefficients together with their standard deviations. Based on these values, the conversion into distance values is performed.

However, a correction is needed as the deformation of the sensor is induced at the rim of the sensor stack. To correct the effect a factor, which takes into account that by tilting the first contact is happening at the edge of the sensor and the biggest height difference will be between the contact point and the opposite side (**Figure 5**).

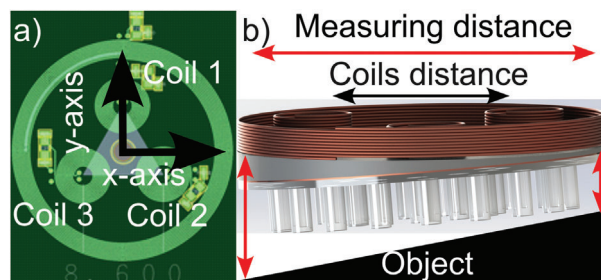


Figure 5. Visualization of the coil placement and scaling effect for triangulation.

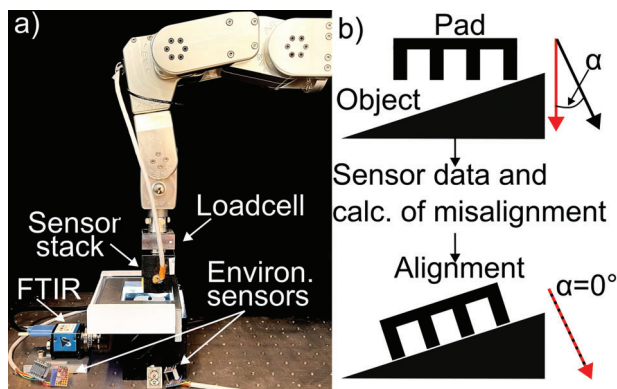


Figure 6. Experimental setup to characterize the sensor system and workflow of the misalignment correction. a) Measuring setup with the installed sensor and adhesive pads. The sensor system is attached to the robot with a three-axis load cell between the sensor and the robot itself. For reference measurements of the alignment and the contact area, an optical setup for frustrated total internal reflection (FTIR) measurements is installed. To track environmental factors like humidity, temperature, pressure, and lightning conditions two sensors controlled by an Arduino were also placed inside the robot cell. b) Measuring principle of the sensor stack.

So for correcting the calculated tilting angle a scaling factor is introduced. This scaling factor (Equation (2)) takes the ratio of the diameter of the measuring layer and the transmitter coil (24 mm) to the distance of the receiver coils.

$$\text{scaling Factor} = \frac{\text{Meas. distance}}{\text{Coils distance}} = \frac{24 \text{ mm}}{8.6 \text{ mm}} = 2.79 \quad (2)$$

The calculated misalignment angle is divided by the scaling factor to obtain the correct angle value.

2.3. Detection of Misalignment and Sensor Validation

The misalignment experiments were carried out with the adhesion setup in the robot cell (Figure 6a) to enable precise and reproducible tilting of the pad around the different axis of the robot (for detailed explanation see Section 5 (Experimental Section): setup for the tilt measurements). Figure 6b illustrates the measurement principle and the goal of the study which is to develop a sensor to measure misalignment angles between the current normal vector of the object (black) and the nominal vector of the pad (red) to perform alignment correction.

To validate the capabilities of the sensor, four different tilt settings are selected. The system is tilted around the x - and y -axis in negative and positive directions (Figure 5). The sensor stack is stepwise pressed against a flat glass substrate.

2.3.1. Sensor Performance

Figure 7 shows the calculated angle for each step for a 1 degree tilting with corresponding contact images for selected steps and positive tilting around the y -axis.

The calculated tilting angles show a convergence over the steps as shown in Figure 7. Over the first few steps, the predicted misalignment angle is increasing because the pad has not enough contact to deform the measuring layer sufficiently. To determine the point of evaluation for the calculated angle the slope between

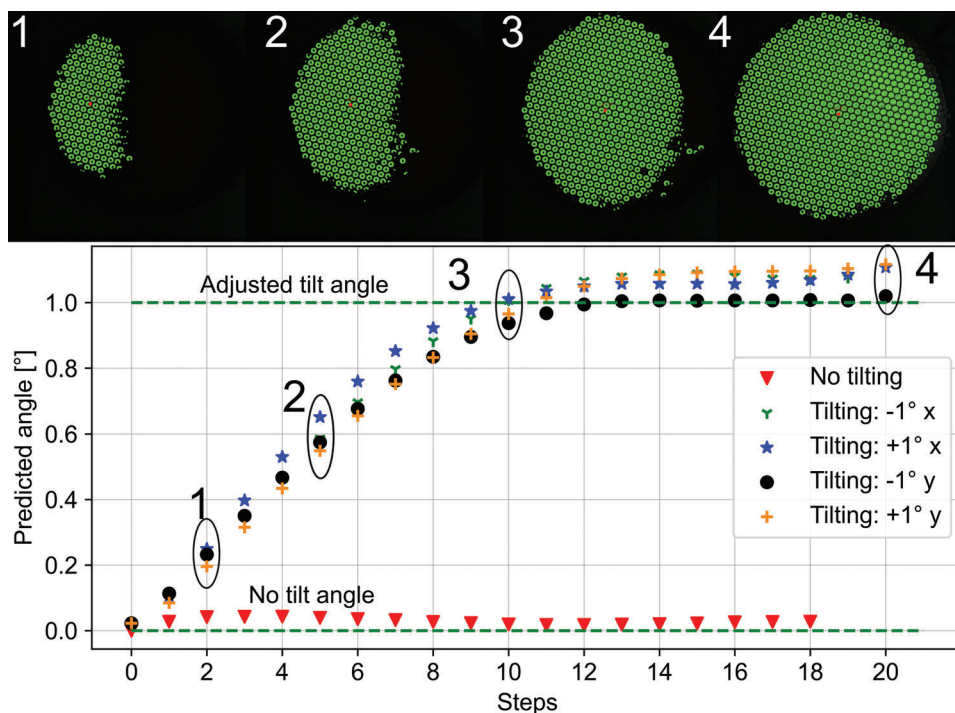


Figure 7. Tilt angle over steps for every tilt configuration. Exemplary contact images for positive tilting around the y -axis added to illustrate the contact formation with increasing step count.

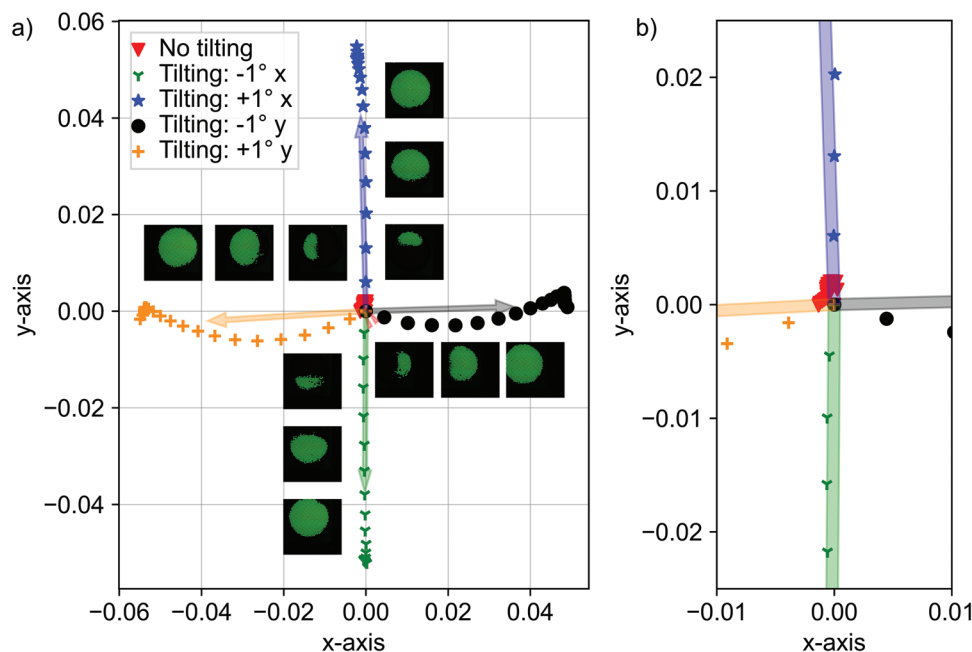


Figure 8. Tilt axis detection for planar glass object with tilting around x - and y -axis in positive and negative direction. a) Overview of all five different tilting angle experiments including contact images. The arrows show the mean direction of each experiment. b) Magnified view of the results around the origin to magnify the experiment without tilting.

the consecutive steps is calculated. At a critical point the slope shows an inflection point which is defined as the point to evaluate the angle. In addition to pure detection of the tilt angle, the tilt axis can also be found out by projecting the determined plane vector to the x - y plane. **Figure 8a** shows the projection of the vector in the x - y plane for each step. For visualization purposes, an arrow of the mean direction of each measurement is added and a zoom view is shown **Figure 8b**.

The sensor stack was manually attached so that the tilt axes of the robot should match the axes of the sensor as closely as possible. As can be seen in **Figure 8**, the tilt axis can be determined with sufficient accuracy after the first contact, and it converges to the x - and y -axes in subsequent steps.

2.3.2. Misalignment Detection

In order to test the capabilities of the sensor system, five different tilt angle classes in compression were considered. In all measurements, the vector in the aligned state is taken as reference, since only relative angle changes are considered. The vector in the aligned state is understood to be the averaged direction vector after the auto alignment.

In **Table 4** and **5** the calculated angles for tilting around the x - and y -axis are summarized, each test is repeated three times for testing the reproducibility of the prediction.

The largest deviation from the set angle is around 0.1 degree. The average deviation from the target angles is 0.042 degree and thus the sensor system achieves a high accuracy. The predicted angles show a linear progression with low standard deviation both in x and y -direction, which confirms a reliable prediction capability (**Figure 9**).

Table 4. Angle evaluation for tilting around the y -axis.

Adjusted tilt angle [degree]	-1.00	-0.80	-0.60	-0.40	-0.20	0.20	0.40	0.60	0.80	1.00
Calculated angle [degree]	-1.07	-0.87	-0.65	-0.43	-0.20	0.20	0.39	0.62	0.81	1.01
Std. Dev. of calculated angle [degree]	0.02	0.01	0.02	0.02	0.01	0.02	0.02	0.02	0.01	0.01

Table 5. Angle evaluation for tilting around the x -axis.

Adjusted tilt angle [degree]	-1.00	-0.80	-0.60	-0.40	-0.20	0.20	0.40	0.60	0.8	1.0
Calculated angle [degree]	-1.07	-0.83	-0.65	-0.43	-0.14	0.23	0.43	0.65	0.90	1.09
Std. Dev. of calculated angle [degree]	0.02	0.01	0.01	0.02	0.01	0.02	0.03	0.05	< 0.01	0.05

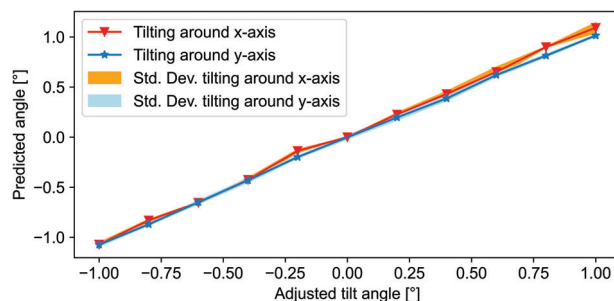


Figure 9. Predicted versus adjusted tilt angle for tilting the sensor around the x -axis (red) and for tilting the sensor around the y -axis (blue).

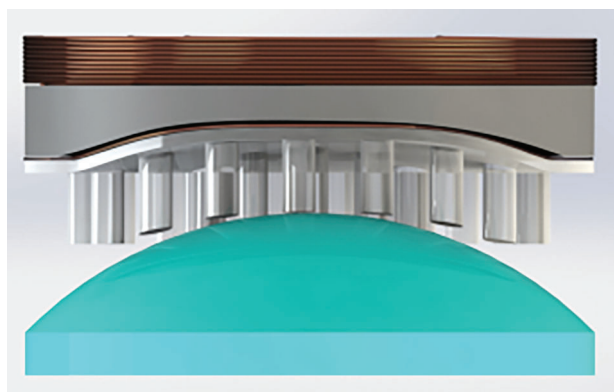


Figure 10. Schematic structure of the experiment for lenticular objects.

The results indicate that the sensor stack is suitable for precise detection of misalignment and fast identification of misalignment direction for flat objects. As the sensor only exhibits three sensing coils and misalignment is approximated by triangulation, predictions will be less accurate when the objects exhibit more complex topography. To evaluate this effect and explore the limits of the sensor concept, contact and misalignment experiments were repeated on a glass lens.

2.4. Sensor Limitations

To test the limitations of the developed sensor stack, the sensor is tested on a curved lens with a radius of 39.1 mm to check the prediction accuracy and the prediction itself (**Figure 10**). For this purpose, the sensor is first aligned on a straight glass plate and then applied to the lens. Subsequently, tilting experiments with a misalignment angle of 1 degree are conducted for all four directions similarly to the experiments described in the Experimental Section (Misalignment measurement procedure).

In the aligned state, a parallel plane should theoretically result because the peak of the lens should get in contact with the middle of the sensor first and a radial displacement be applied to the sensor around the center. The predicted tilting angle could indicate that the highest point of the lens and the center of the sensor were not aligned perfectly during the measurement. In addition, it demonstrates that, as could be expected, the prediction using triangulation does not extend to nonplanar surfaces.

In **Table 6** the calculated angles from the measurement with a lenticular specimen are shown. The predicted angles were on average 0.48 degree for the aligned experiments and between 1.49 and 2.79 degree for tilting experiments with a tilting angle of 1 degree.

In addition to calculating the tilt angle, the ability of the sensor to correctly predict the tilt direction in this scenario must be tested. **Figure 11** visualizes the calculated directions. The tilting axis is still predictable even if the shape of the object is curved,

especially when it is taken into consideration that the lens was only placed manually below the gripper.

3. Conclusion

In this paper, we presented a concept for a coil-based sensor capable of detecting small misalignments during the attachment of a bioinspired adhesive surface. The sensor consists of a stack of three different components:

- 1) PCB-based sensor coils
- 2) Deformable flexible support material
- 3) Conductive flexible measuring layer

An optimized sensor stackable to detect a tilt of just ± 0.042 degrees on average was implemented. In addition to the measurement of the absolute angle, the tilt axis could also be detected reliably shortly after the first contact. Considering the precision of the conventional manual adjustment, this represents a promising approach to speed up adhesion measurements in laboratories and improve industrial robot-based gripping processes, without affecting the gripping ability of the system.

Common pick-and-place tasks could thus be processed in a more reliable, modular, and faster way since no manual alignment of the gripping system is necessary. This opens more versatile application possibilities, as the gripping system can adapt automatically to new gripping scenarios. Additionally, the sensor system can improve the quality of novel experiments in the laboratory where alignment is still very challenging. Thus far, systems like the optical FTIR setup used as reference in this work enable the alignment of translucent, flat substrates and to the best of the authors knowledge no comparable in situ methods exist to align non-transparent samples.

In the future, the sensor system can be expanded to include other variables, such as a prediction of the contact pressure. If possible, this should not be predicted integrally, but rather locally, to provide an estimate of the contact area and contact quality. With this information, it is possible to realize optimal approach trajectories by using the maximum contact force, resulting in the highest possible adhesive force. Also, the prediction of object properties, such as shape, stiffness, or weight is a promising goal for industrial as well as lab-scale applications. These values would serve as input information for robot control, whereby an auto-adaptive control can be implemented and bioinspired grippers could become more extensively used in industrial pick-and-place applications.

4. Experimental Section

Adhesive Pads: The adhesive pads had a diameter of 24 mm. On each pad, ≈ 816 cylindrical pillars with a diameter of 0.4 mm were distributed in a regular hexagonal shape. For the development and testing of the sensor, the tips of the pillars were not modified to increase adhesion forces as

Table 6. Calculated misalignment angles for a lenticular specimen.

Adjusted tilt angle [degree]	-1 around x-axis	1 around x-axis	0	1 around y-axis	-1 around y-axis
Calculated angle [degree]	1.49	1.68	0.48	2.79	2.75

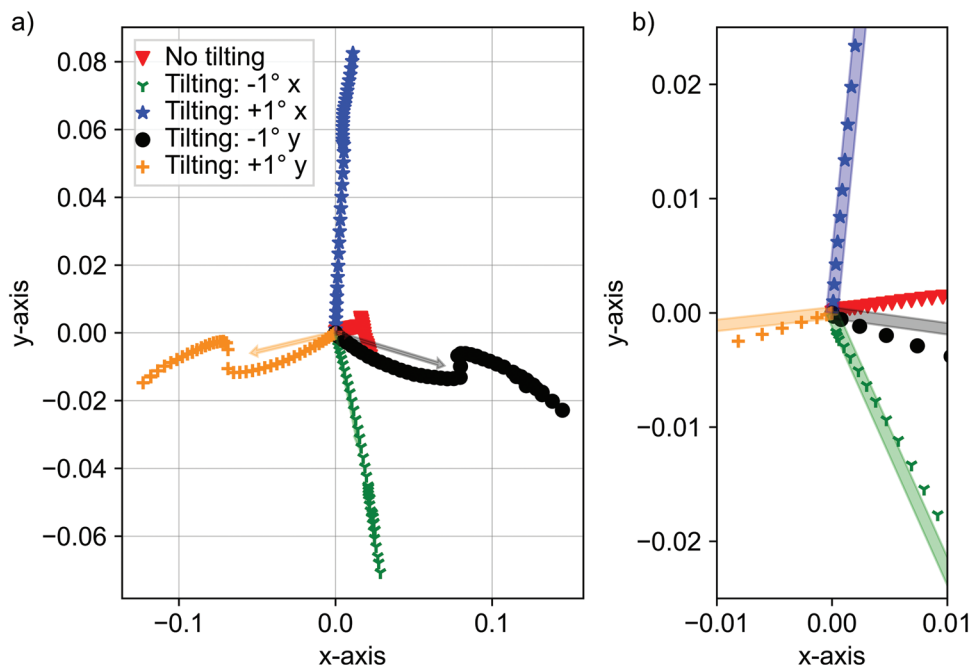


Figure 11. Tilt axis detection for lenticular glass object with tilting around x- and y-axis in positive and negative direction. a) Overview of all five different tilting angle experiments. The arrows show the mean direction of each experiment. b) Magnified view of the results around the origin to magnify the experiment without tilting.

all experiments were carried out in the compressive regime to reduce the experimental procedure's time. Just for testing the influence of the conductive measuring layer on the adhesion force modified pillars were used. The bioinspired specimens were provided by Innocise GmbH.

Sensor Stack: The tactile sensor consists of different elements attached to the adhesive pad (Figure 1): The sensor consists of a sensor layer composed of transmitter and receiver coils. A flexible and deformable layer followed this. Finally, a conductive measuring layer allowed the excitation of eddy currents. More information regarding these components will be provided in the subsequent sections.

Sensing Layer: The sensing layer consists of one transmitter coil with a diameter of 24 mm surrounding three identical receiver coils with a diameter of 6 mm each. The geometrical parameters of the coils were limited by the footprint of the adhesive pad with a diameter of 24 mm. Inside the transmitter coil, the three receiver coils were placed on an equilateral triangle inscribed in a circle. The sensor was integrated on a PCB. The E-CAD (electronic computer-aided design) design was realized via ECadstar (2022.0). They were manufactured by Würth Elektronik GmbH & Co KG. An impedance analyzer (Keysight E4990A) and network analyzer (Agilent 4395A) were used for characterizing the coils' properties. As a commercially available LAN cable connected the coil to the circuit board.

Deformable Layer: The foam acted as a supporting structure between the coils and the measuring layer to improve contact to surfaces due to its compliance. The deformation of the foam itself should had no impact on the measurement system therefore, foams with fast relaxation were advantageous. In this study, five commercially available foams are investigated, as listed in Table 7.

Measuring Layer: Commercially available conductive sheets were tested as measuring layer materials to achieve an optimal signal quality without affecting the adhesion force. The conductivity of the material should be as high as possible for effective eddy current excitation with a mechanical behavior similar to the foam used as a supporting structure. The materials were prescreened based on these properties and three specimens were selected as listed in Table 8.

The materials were characterized by evaluating the signal amplitude of the sensor. For this purpose, the sensor was placed at an equal distance

Table 7. List of tested foam specimens with their corresponding manufacture.

Foam	Manufacture
M Foam	3M
GT 7116	3M
4229 P	3M
PT1500	3M
KS 865 F	Klebeschop24

Table 8. Measuring layer materials, *reference material.

Measuring layer material	Manufacturer
3304 BCS	3M
ECATT9711S-200	3M
Shieldex Kassel	Statex Produktions- und Vertriebs GmbH
Copper foil*	Bürklin (distributor)

above the measuring layer material and then the coil was moved stepwise by 40 μm toward the measuring layer material, ten steps were performed.

Measuring Setup: In this study, two different measurement setup configurations were used; one arrangement was used to characterize the mechanical properties of the constituent components and their interaction with one another, while the second setup was used to examine the sensor's capacity to detect tilting.

Setup for the Mechanical Characterization of the Different Parts: For testing the mechanical properties of the sensor components individually and collectively, manipulation system with a 200 N load cell (KD40S ME-Meßsysteme GmbH) was used. For aligning the pad an optical setup

leveraging the principal of FTIR inspired by previous publications by Tinnemann et al. was integrated in the setup.^[2,34,35]

Mechanical properties of the foam in terms of hysteresis and deformation behavior and the influence of the measuring layer material on the adhesive force were investigated with this setup. A set of tests was carried out on the samples to characterize them. In each test the samples were subjected to 50 load cycles between ± 100 N, therefore the foam was glued between a metallic carrier and a plexiglass plate. For evaluating the influence of the measuring layer material on the adhesion force a comparison between the adhesion force of the following four configuration was done:

- 1) Pad
- 2) Pad with foam as support structure
- 3) Pad with measuring layer material
- 4) Pad with foam and measuring layer material

The adhesion force of the pads was tested on a flat glass substrate, which was attached to a goniometer enabling a parallel alignment. The test velocity was set to $0.017 \text{ mm}^{-1} \text{ s}$ and the preload for the test was set to 15 N for each configuration the experiment was repeated twenty times. For each configuration, a separate pad (with modified tip geometry) was used.

Setup for the Tilt Measurements: The measurement setup was integrated in a robot cell. The robot (Meca 500, Mecademic) enabled precise and reproducible manipulation of the sensor stack together with the adhesive pad. Behind the adhesive pad a three-axis load cell with ± 50 N (K3D40 ME-Meßsysteme GmbH) was installed to measure the force and determine the first contact between the pad and glass substrate. Within the robot cell an optical setup visualized the contact pattern of the pad via the FTIR principal. The camera used for image capturing is a DFK 23UP031 equipped with TPL 0820 7MP lens from The Imaging Source Europe GmbH. For operating the sensor a STEMLab 125-14 (red pitaya) was utilized. A custom-written bit file was implemented on the field programmable gate array (FPGA) to handle the signal generation as well as the data acquisition and multiplexing the signals from the three receiver coils. A custom-built circuitry was linked between the red pitaya board and the sensor to control the amplification of every coil and to demodulate the received signals in order to achieve the best signal to noise ratio (SNR). After this, the amplitude was calculated via Equation (3)

$$\text{Amplitude} = \sqrt{I^2 + Q^2} \quad (3)$$

In Equation (3) I and Q are the demodulated signals received for each coil. To eliminate the influence of absolute values the difference of the amplitude was calculated. This means that the amplitude value in the relaxed (unloaded) state was subtracted from all other values, so that a zero signal was present in the unloaded state.

Misalignment Measurement Procedure: Quantification of misalignment was a central aspect of this study. However, in practice, there were no tools to measure it in situ. Therefore, an auto-alignment procedure based on the optical contact images from FTIR was developed to ensure reproducible alignment conditions for the sensor tests (see Supporting Information). In order to then carry out the tilt measurements, the robot moved in $40 \mu\text{m}$ steps onto a glass plate until a force of 20 N was reached. The robot was always moved straight onto the glass once (in the aligned state). Afterward, the pad was tilted by a defined angle around each axis in the positive and negative direction and the above procedure was carried out each time. Tilt angles varied from 0 to 1 degree in 0.2 degree steps and each measurement was repeated three times.

Software: A custom-written software in Python (Version 3.10.5) controlled all measuring devices and synchronized all data acquisition steps. For each measuring device (load cell, camera, sensor, robot) an individual python script was handling the data acquisition and data storing. The communication between the different processes enabled the triggering of measurements and the highly precise data synchronization. A separate vir-

tual environment was used for data analysis and data visualization, which was based on Python version 3.8.8.

Statistical Section: In the following section information regarding the analysis is provided. Data preprocessing: Lowpass filtering was applied to the raw signals. Additionally the signals were offset shifted to be only positive and the signal amplitude was calculated. For analysis, differential signals between unloaded and loaded state were calculated. Sensors were calibrated using the method described in the publication. Data presentation: Continuous variables were given as the mean value of the samples, standard deviation ($\pm 1\text{SD}$) were provided in tables and in specific diagrams. Sample size: Five different tilting configuration with five different angles were tested stepwise with ≈ 20 steps for each configuration. All measurements were repeated three times, resulting in ≈ 1500 angle evaluations. Software used for statistical analysis: Python was used throughout the whole analysis.

Supporting Information

Supporting Information is available from the Wiley Online Library or from the author.

Acknowledgements

S.H. thanks Jonathan Thiemecke (Innocise GmbH) for his support in performing the adhesion tests as well as preparing the samples and Marius Schäfer (Fraunhofer IZFP) for his help in building the bit file for the FPGA. NEXT.robotics GmbH & Co.KG is acknowledged for providing the robot within the GeckI research project. S.H. and S.C.L.F. also thank their colleagues Michael M. Becker and Martin Schuppmann (Fraunhofer IZFP) for fruitful discussions. This research was funded by Federal Ministry of Education and Research as part of the project number 01IS21035B as well as partially funded by a Fraunhofer Internal Program under the Grant No. Attract 025-601314 awarded to S.C.L Fischer.

Open access funding enabled and organized by Projekt DEAL.

Conflict of Interest

The authors declare no conflict of interest.

Author Contributions

S.H., P.S., and S.C.L.F. conceptualized the idea. S.H. and P.S. designed the methodology and performed the investigation. S.H. performed the formal analysis, did the visualization, developed the software, and wrote the original draft. S.C.L.F. did the funding acquisition. S.C.L.F. supervised the study. Writing-review and editing: S.H. and S.C.L.F. wrote, reviewed, and edited the final manuscript. All authors read and agreed to the published version of the manuscript

Keywords

bioinspired adhesive gripping systems, eddy currents, robotics, sensor development

Received: June 19, 2023
Revised: August 28, 2023
Published online:

[1] E. Arzt, S. Gorb, R. Spolenak, *Proc. Natl. Acad. Sci. USA* **2003**, *100*, 10603.

- [2] L. Barnefske, F. Rundel, K. Moh, R. Hensel, X. Zhang, E. Arzt, *Adv Materials Interfaces* **2022**, 9, 2201232.
- [3] E. Arzt, H. Quan, R. M. McMeeking, R. Hensel, *Prog. Mater. Sci.* **2021**, 120, 100823.
- [4] S. Kim, M. Sitti, *Appl. Phys. Lett.* **2006**, 89, 261911.
- [5] R. G. Balijepalli, S. C. Fischer, R. Hensel, R. M. McMeeking, E. Arzt, *J. Mech. Phys. Solids* **2017**, 99, 357.
- [6] S. C. L. Fischer, E. Arzt, R. Hensel, *ACS Appl. Mater. Interfaces* **2017**, 9, 1036.
- [7] V. Tinnemann, L. Hernández, S. C. L. Fischer, E. Arzt, R. Bennewitz, R. Hensel, *Adv. Funct. Mater.* **2019**, 29, 1807713.
- [8] D. Son, V. Liimatainen, M. Sitti, *Small* **2021**, 17, e2102867.
- [9] S. C. L. Fischer, K. Groß, O. Torrents Abad, M. M. Becker, E. Park, R. Hensel, E. Arzt, *Adv. Mater. Interfaces* **2017**, 4, 1700292.
- [10] M. P. Murphy, S. Kim, M. Sitti, *ACS Appl. Mater. Interfaces* **2009**, 1, 849.
- [11] R. Hensel, K. Moh, E. Arzt, *Adv. Funct. Mater.* **2018**, 28, 1800865.
- [12] M. Bacca, J. A. Booth, K. L. Turner, R. M. McMeeking, *J. Mech. Phys. Solids* **2016**, 96, 428.
- [13] J. A. Booth, M. Bacca, R. M. McMeeking, K. L. Foster, *Adv. Mater. Interfaces* **2018**, 5, 1800272.
- [14] R. G. Balijepalli, M. R. Begley, N. A. Fleck, R. M. McMeeking, E. Arzt, *Int. J. Solids Struct.* **2016**, 85–86, 160.
- [15] E. Kroner, D. R. Paretkar, R. M. McMeeking, E. Arzt, *J. Adhes.* **2011**, 87, 447.
- [16] D. Wang, H. Tian, H. Liu, J. Zhang, H. Hu, X. Li, C. Wang, X. Chen, J. Shao, *Adv. Sci.* **2023**, 10, 2302512.
- [17] T. Y. Kim, W. Suh, U. Jeong, *Mater. Sci. Eng.: R: Rep.* **2021**, 146, 100640.
- [18] H. Wang, D. Jones, G. de Boer, J. Kow, L. Beccai, A. Alazmani, P. Culmer, *IEEE Sens. J.* **2018**, 18, 7793.
- [19] H. Wang, J. Kow, N. Raske, G. de Boer, M. Ghajari, R. Hewson, A. Alazmani, P. Culmer, *Sens. Actuators, A* **2018**, 271, 44.
- [20] H. Wang, M. Totaro, S. Veerapandian, M. Ilyas, M. Kong, U. Jeong, L. Beccai, *Adv. Mater. Technol.* **2020**, 5, 2000659.
- [21] W. Yuan, S. Dong, E. H. Adelson, *Sensors* **2017**, 17, 2762.
- [22] S. Gast, K. Zimmermann, *J. Sens. Sens. Syst.* **2020**, 9, 319.
- [23] C. Pang, K. Mak, Y. Zhang, Y. Yang, Y. A. Tse, M. Y. Wang, presented at *2021 IEEE International Conference on Robotics and Automation (ICRA)*, Xi'an, China, May **2021**.
- [24] C. Pang, Q. Wang, K. Mak, H. Yu, M. Y. Wang, *IEEE Robot. Autom. Lett.* **2022**, 7, 7842.
- [25] H. Wang, G. de Boer, J. Kow, A. Alazmani, M. Ghajari, R. Hewson, P. Culmer, *Sensors* **2016**, 16, 1356.
- [26] G. de Boer, N. Raske, H. Wang, J. Kow, A. Alazmani, M. Ghajari, P. Culmer, R. Hewson, *Sensors* **2017**, 17, 2539.
- [27] M. Neto, P. Ribeiro, R. Nunes, L. Jamone, A. Bernardino, S. Cardoso, *Sensors* **2021**, 21, 5098.
- [28] H. Wang, J. Kow, G. de Boer, D. Jones, A. Alazmani, P. Culmer, in *IEEE SENSORS 2017: October 29–November 1, 2017, Glasgow, Scotland, UK, Scottish Event Campus (SEC) 2017 conference proceedings* (Ed.: I. SENSORS), IEEE, Piscataway, NJ **2017**, p. 1.
- [29] X. A. Wu, S. A. Suresh, H. Jiang, J. V. Ulmen, E. W. Hawkes, D. L. Christensen, M. R. Cutkosky, presented at *2015 IEEE/RSJ International Conference on Intelligent Robots and Systems (IROS)*, Hamburg, Germany, September **2015**, p. 1501.
- [30] X. A. Wu, D. L. Christensen, S. A. Suresh, H. Jiang, W. R. T. Roderick, M. Cutkosky, *IEEE Robot. Autom. Lett.* **2017**, 2, 460.
- [31] J.-P. Roberge, W. Ruotolo, V. Duchaine, M. Cutkosky, *IEEE Robot. Autom. Lett.* **2018**, 3, 1041.
- [32] T.-H.-L. Le, A. Maslyczyk, J.-P. Roberge, V. Duchaine, in *IEEE International Conference on Robotics and Automation (ICRA)*, Singapore, May **2017**, p. 407.
- [33] J. Hashizume, T. M. Huh, S. A. Suresh, M. R. Cutkosky, *IEEE Robot. Autom. Lett.* **2019**, 4, 677.
- [34] M. Samri, J. Thiemecke, E. Prinz, T. Dahmen, R. Hensel, E. Arzt, *Mater. Today* **2022**, 53, 41.
- [35] R. Hensel, J. Thiemecke, J. A. Booth, *ACS Appl. Mater. Interfaces* **2021**, 13, 19422.



Simon Herter graduated from Saarland University in 2020 with a Master of Science degree in materials science. He is currently pursuing a Ph.D. within the MatBeyoNDT research group at Fraunhofer IZFP (and the lab for measurement technology at Saarland University). His work focuses on the development of sensors and algorithms specifically with regard to bioinspired adhesive structures. He is particularly interested in inductive sensors and machine learning methods in order to develop simple but powerful sensors for complex tasks.



Philipp Stopp graduated from the University of Applied Sciences in Saarbrücken in 2015 with a Master of Science degree in electrical engineering majoring in microelectronics and telecommunication. He is currently a research associate at Fraunhofer IZFP in the competence area “Sensor Intelligence and Microelectronics”. His work focuses on the development and implementation of miniaturized sensor electronics for industrial measurement equipment and IoT devices.



Sarah Fischer is currently Head of the Research Group MatBeyoNDT at Fraunhofer IZFP in Germany. After earning a Ph.D. in Materials Science in the area of bioinspired adhesive surfaces, she joined Apple’s polymer engineering team in California to work on industrial applications of adhesives. After 1.5 years, she moved back to Germany to build her own research group at Fraunhofer IZFP and develop innovative experimental mechanics methods for complex materials at the interface of research and industry.